
A DOMAIN SPLITTING STRATEGY FOR SOLVING PDES

Ken Trotti

Faculty of Informatics
University of Italian Switzerland
ken.trotti@usi.ch

March 3, 2023

ABSTRACT

In this work we develop a novel domain splitting strategy for the solution of partial differential equations. Focusing on a uniform discretization of the d -dimensional advection-diffusion equation, our proposal is a two-level algorithm that merges the solutions obtained from the discretization of the equation over highly anisotropic submeshes to compute an initial approximation of the fine solution. The algorithm then iteratively refines the initial guess by leveraging the structure of the residual. Performing costly calculations on anisotropic submeshes enable us to reduce the dimensionality of the problem by one, and the merging process, which involves the computation of solutions over disjoint domains, allows for parallel implementation.

Keywords partial differential equations · advection-diffusion equation · Richardson extrapolation · domain splitting · parallel in time integration

1 Introduction

Supercomputer nowadays are high-performance computers with thousands and even millions of cores, that are designed to handle extremely large and complex computing tasks. This makes parallelization, or the ability to divide a task into smaller parts that can be run simultaneously on different cores, an important factor in maximizing the performance of a supercomputer. To effectively exploit this feature, an algorithm must be designed accordingly. In the case of high-dimensional partial differential equations, there are several standard approaches. These include Deep Learning techniques [6, 7, 11], Monte Carlo methods [20, 19], Sparse grids [1], and other methods consists in exploiting properties of the domain, symmetries, regularity, see e.g. [12].

The Sparse Grids (SG) method starts with a uniform mesh with N^d grid points and then removes certain points according to a specific rule, yielding a sparse mesh with $O(N \log^{d-1} N)$ grid points. While this approach allows for low memory requirements, it also leads to an increased approximation error compared to using a uniform mesh. Specifically, when a second-order accurate scheme is used, the resulting approximation error in the L^2 norm is $O(N^{-2} \log(N)^{d-1})$, which is larger than the error of $O(N^{-2})$ achieved with the uniform mesh.

Our goal is to develop an approach that utilizes a coarser mesh than a uniform one, but avoids the increase in error that is characteristic of SG. Therefore, we aim to develop an algorithm that allows for efficient and parallel computation while maintaining a high level of accuracy and potentially low memory requirements. To achieve this goal, we introduce the *Anisotropic Submeshes Domain Splitting Method* (ASDSM), a novel two-level domain splitting method for the parallel solution of d -dimensional PDEs. ASDSM involves dividing a fine uniform mesh into multiple strongly anisotropic submeshes. The solutions obtained from each submesh are then merged together forming an approximate solution of the discretized PDE on the uniform mesh. The process is repeated by exploiting the structure of the residual to improve the accuracy of the solution. This approach allows us to effectively reduce the dimensionality of the problem by a factor of one, allowing for the efficient solution of larger and more complex problems. Additionally, as discussed in Section 3.3 a smart memory handling strategy can further reduce the memory requirements compared to using the original uniform mesh.

In this preliminary research, we focus on the well-known advection-diffusion equation, which is a fundamental mathematical model used in a variety of fields including fluid dynamics, heat transfer, and contaminant transport [3, 16, 13].

Consider the following d -dimensional advection-diffusion equation with Dirichlet boundary conditions (BCs)

$$\begin{cases} -\sum_{i=1}^d \alpha_i \frac{\partial u}{\partial x_i^2}(\mathbf{x}) + \beta_i \frac{\partial u}{\partial x_i}(\mathbf{x}) = s(\mathbf{x}), & \mathbf{x} \in \Omega \subset \mathbb{R}^d, \\ u(\mathbf{x}) = g(\mathbf{x}), & \mathbf{x} \in \partial\Omega, \end{cases} \quad (1)$$

and its time-dependent counterpart

$$\begin{cases} \frac{\partial u}{\partial t}(\mathbf{x}, t) - \sum_{i=1}^d \alpha_i \frac{\partial u}{\partial x_i^2}(\mathbf{x}) + \beta_i \frac{\partial u}{\partial x_i}(\mathbf{x}) = s(\mathbf{x}, t), & (\mathbf{x}, t) \in \Omega \times [0, 1] \subset \mathbb{R}^{d+1}, \\ u(\mathbf{x}) = g(\mathbf{x}, t), & (\mathbf{x}, t) \in \partial\Omega \times [0, 1), \end{cases} \quad (2)$$

where s is the source term, g the BCs, $\alpha > 0$ the diffusion coefficient, β the velocity field and Ω the space domain.

In the following sections, we will provide a detailed description of ASDSM. In details, in Section 2 we introduce the basic tools needed to explain ASDSM. We provide the detailed construction of the involved meshes and projectors, and briefly sum up the discretization process of the PDE. In Section 3, we provide a step-by-step explanation with figures to illustrate the ASDSM Algorithm. We also provide some remarks on how to implement the algorithm efficiently. In Section 4, we present numerical results demonstrating the effectiveness of our method in terms of residual reduction per iteration. Finally, in Section 5, we draw conclusions and outline potential areas for future work. We discuss the implications of our method and how it can be applied to other problems in the field.

2 Introduction to the ASDSM Algorithm

For the sake of simplicity, in this section we will consider the two-dimensional case of the PDE in (1) on the square domain $\Omega = [0, 1] \times [0, 1]$.

Before providing the ASDSM Algorithm, we first introduce the necessary meshes and fix the notation. We then discretize the PDE using the finite differences method, and introduce the projectors that will be used to project the unknown onto different meshes. These tools form the foundation upon which the ASDSM Algorithm is built, and will be essential for understanding the details of the method.

2.1 Meshes

Let $N_c^{(x)}, N_f^{(x)}, N_c^{(y)}, N_f^{(y)} \in \mathbb{N}$ such that

$$\begin{aligned} N_f^{(x)} + 1 &= n_x(N_c^{(x)} + 1), \\ N_f^{(y)} + 1 &= n_y(N_c^{(y)} + 1), \end{aligned} \quad (3)$$

for some $n_x, n_y \in \mathbb{N}$. Then consider the step lengths

$$\begin{aligned} h_x &= \frac{1}{N_f^{(x)} + 1}, & h_y &= \frac{1}{N_f^{(y)} + 1}, \\ H_x &= \frac{1}{N_c^{(x)} + 1} = n_x h_x, & H_y &= \frac{1}{N_c^{(y)} + 1} = n_y h_y, \end{aligned} \quad (4)$$

and the following uniform meshes

$$\begin{aligned} \Omega^{h_x, h_y} &= \{(x_i, y_j) \mid x_i = ih_x, y_j = jh_y, i = 1, \dots, N_f^{(x)}, j = 1, \dots, N_f^{(y)}\}; \\ \Omega^{h_x, H_y} &= \{(x_i, y_j) \mid x_i = ih_x, y_j = jH_y, i = 1, \dots, N_f^{(x)}, j = 1, \dots, N_c^{(y)}\}; \\ \Omega^{H_x, h_y} &= \{(x_i, y_j) \mid x_i = iH_x, y_j = jh_y, i = 1, \dots, N_c^{(x)}, j = 1, \dots, N_f^{(y)}\}; \\ \Omega^{H_x, H_y} &= \{(x_i, y_j) \mid x_i = iH_x, y_j = jH_y, i = 1, \dots, N_c^{(x)}, j = 1, \dots, N_c^{(y)}\}; \\ \Omega_{i,j}^{h_x, h_y} &= \left\{ (x_k, y_l) \mid \begin{array}{l} x_k = iH_x + kh_x, \quad k = 1, \dots, n_x - 1, \quad i = 0, \dots, N_c^{(x)} \\ y_l = jH_y + lh_y, \quad l = 1, \dots, n_y - 1, \quad j = 0, \dots, N_c^{(y)} \end{array} \right\}. \end{aligned} \quad (5)$$

We will refer to the meshes in equation (5) respectively as the fine mesh, the anisotropic meshes dense along the x and y axis, the coarse mesh and the ‘‘holes’’. Moreover, the union between $\Omega^{h_x, H_y} \cup \Omega^{H_x, h_y}$ is called *skeleton* or *coarse structure*. Furthermore, we denote by $\Omega_{holes}^{h_x, h_y}$ the union of all holes, i.e. $\Omega_{holes}^{h_x, h_y} := \cup_{i,j=0}^{N_c^{(x)}, N_c^{(y)}} \Omega_{i,j}^{h_x, h_y}$.

The following proposition, which is a consequence of the condition in equation (3), shows the relations between the meshes in (5).

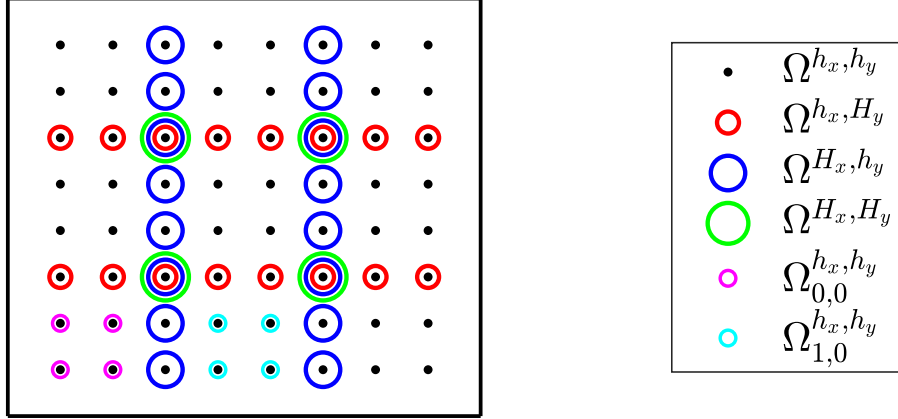


Figure 1: Graphical representation of the meshes.

Proposition 2.1. Consider the meshes in equation (5), then the following relations hold

- $\Omega^{h_x, H_y} \subset \Omega^{h_x, h_y}, \quad \Omega^{H_x, h_y} \subset \Omega^{h_x, h_y};$
- $\Omega^{H_x, H_y} \subset \Omega^{h_x, h_y}, \quad \Omega^{H_x, H_y} \subset \Omega^{H_x, h_y}, \quad \Omega^{H_x, H_y} \subset \Omega^{h_x, H_y};$
- $\Omega_{i,j}^{h_x, h_y} \cap \Omega_{k,l}^{h_x, h_y} = \emptyset$ if $(i, j) \neq (k, l);$
- $\Omega_{holes}^{h_x, h_y} = \Omega^{h_x, h_y} \setminus (\Omega^{h_x, H_y} \cup \Omega^{H_x, h_y}).$

In Proposition 2.1, item (a) show that the two anisotropic meshes are sub-meshes of the fine one, and item (b) shows that the coarse mesh is a sub-mesh of the fine mesh and the anisotropic meshes. Moreover, from item (a) it follows that the mesh $\Omega^{h_x, H_y} \cup \Omega^{H_x, h_y}$ is a *non-uniform* sub-mesh of the fine one from which, by adding $\Omega_{holes}^{h_x, h_y}$, we obtain the fine mesh.

Indeed, equivalently to item (d), we have

$$\Omega^{h_x, h_y} = \left(\bigcup_{i,j=0}^{N_c^{(x)}, N_c^{(y)}} \Omega_{i,j}^{h_x, h_y} \right) \cup \Omega^{h_x, H_y} \cup \Omega^{H_x, h_y}.$$

Let $N_c^{(x)} = N_c^{(y)} = 2$, $N_f^{(x)} = N_f^{(y)} = 8$. Then Figure 1 shows a graphical representation of the meshes in equation (5).

2.2 Projectors

The ASDSM Algorithm aims to compute the discrete fine solution by solving equations over coarser meshes. In order to do this, we need to introduce the projectors that will allow us to transfer a discrete function from one mesh to another. These projectors will be essential for accurately transferring information between the different meshes used in our method.

We begin by introducing the set of all discrete functions defined over the fine mesh Ω^{h_x, h_y} , in equation (5), as $V^{h_x, h_y} = \{v \mid v \in \mathbb{R}^{\#\Omega^{h_x, h_y}}\}$. Consider $v \in V^{h_x, h_y}$ to be an ordered vector

$$v = [v_{1,1}, v_{2,1}, \dots, v_{N_f^{(x)}, 1}, v_{1,2}, \dots, v_{N_f^{(x)}, 2}, \dots, v_{N_f^{(x)}, N_f^{(y)}}]^T,$$

with $v_{i,j}$ being the value of the discrete function v at the grid point $(x_i, y_j) \in \Omega^{h_x, h_y}$. We also define the sets $V^{h_x, H_y}, V^{H_x, h_y}, V^{H_x, H_y}, V_{i,j}^{h_x, h_y}$ with similarly ordered elements.

Remark 2.2. Clearly, for every position m of $v \in V^{h_x, h_y}$ there exist unique indexes $i \in \{1, \dots, N_f^{(x)}\}$ and $j \in \{1, \dots, N_f^{(y)}\}$ such that $v_m = v_{i,j}$ with $(i-1)N_f^{(y)} + j = m$.

Definition 2.3. Let us define the following projectors.

- 1) $P_{ff}^{fc} : V^{h_x, h_y} \rightarrow V^{h_x, H_y}$, as the projector that maps vectors $v \in V^{h_x, h_y}$ into vector $w \in V^{h_x, H_y}$, $w = P_{ff}^{fc}v$, by only keeping the components $v_{i,j}$ with $(x_i, y_j) \in \Omega^{h_x, H_y}$; Formally, from Remark 2.2,

$$\left(P_{ff}^{fc}\right)_{m,n} = \begin{cases} 1 & \text{if } \Omega^{h_x, h_y} \ni (x_{i(m)}, y_{j(m)}) = (x_{i(n)}, y_{j(n)}) \in \Omega^{h_x, H_y}, \\ 0 & \text{otherwise.} \end{cases}$$

- 2) $P_{ff}^{cf} : V^{h_x, h_y} \rightarrow V^{H_x, h_y}$, as the projector that maps vectors $v \in V^{h_x, h_y}$ into vector $w \in V^{H_x, h_y}$, $w = P_{ff}^{cf}v$, by only keeping the components $v_{i,j}$ with $(x_i, y_j) \in \Omega^{H_x, h_y}$;

- 3) $P_{ff}^{cc} : V^{h_x, h_y} \rightarrow V^{H_x, H_y}$, as the projector that maps vectors $v \in V^{h_x, h_y}$ into vector $w \in V^{H_x, H_y}$, $w = P_{ff}^{cc}v$, by only keeping the components $v_{i,j}$ with $(x_i, y_j) \in \Omega^{H_x, H_y}$;

- 4) $P_{ff}^{holes} : V^{h_x, h_y} \rightarrow V_{holes}^{h_x, h_y}$, as the projector that maps vectors $v \in V^{h_x, h_y}$ into vector $w \in V_{holes}^{h_x, h_y}$, $w = P_{ff}^{holes}v$, by only keeping the components $v_{i,j}$ with $(x_i, y_j) \in \Omega_{holes}^{h_x, h_y}$;

Since the transpose of a projector switches domain with codomain, we note that:

- 1) $\left(P_{ff}^{fc}\right)^T = P_{fc}^{ff}$;
- 2) $\left(P_{ff}^{cf}\right)^T = P_{cf}^{ff}$;
- 3) $\left(P_{ff}^{cc}\right)^T = P_{cc}^{ff}$;
- 4) $\left(P_{ff}^{holes}\right)^T = P_{holes}^{ff}$.

This allows us to retrieve the properties listed in Proposition 2.4.

Proposition 2.4. Let I be the identity matrix of the opportune size. Then the projectors defined above have the following properties:

- 1) $P_{ff}^{fc} \left(P_{ff}^{fc}\right)^T = P_{ff}^{fc} P_{fc}^{ff} = I$;
- 2) $P_{ff}^{cf} \left(P_{ff}^{cf}\right)^T = P_{ff}^{cf} P_{cf}^{ff} = I$;
- 3) $P_{ff}^{cc} \left(P_{ff}^{cc}\right)^T = P_{ff}^{cc} P_{cc}^{ff} = I$;
- 4) $P_{ff}^{holes} \left(P_{ff}^{holes}\right)^T = P_{ff}^{holes} P_{holes}^{ff} = I$;
- 5) Every projector has norm-1 and infinity norm equal to 1.

2.3 Discretization

The discretization of the PDE over the uniform meshes in (5) is done through the second order accurate centered finite differences method, and yields the following linear systems.

$$\begin{aligned} A_{ff} u_{ff} &= b_{ff}, & u_{ff} &\in \mathbb{R}^{N_f^{(x)} N_f^{(x)}}; \\ A_{fc} u_{fc} &= b_{fc}, & u_{fc} &\in \mathbb{R}^{N_f^{(x)} N_c^{(x)}}; \\ A_{cf} u_{cf} &= b_{cf}, & u_{cf} &\in \mathbb{R}^{N_c^{(x)} N_f^{(x)}}; \\ A_{cc} u_{cc} &= b_{cc}, & u_{cc} &\in \mathbb{R}^{N_c^{(x)} N_c^{(x)}}; \\ A_{(ij)} u_{(ij)} &= b_{(ij)}, & u_{(ij)} &\in \mathbb{R}^{(n_x-1)(n_y-1)}, \quad i = 1, \dots, n_x - 1, \quad j = 1, \dots, n_y - 1. \end{aligned} \tag{6}$$

In details,

$$\begin{aligned}
A_{ff} &= \alpha \left(I_{N_f^{(y)}} \otimes \left(\frac{1}{h_x^2} L_{N_f^{(x)}} \right) + \left(\frac{1}{h_y^2} L_{N_f^{(y)}} \right) \otimes I_{N_f^{(x)}} \right) + \\
&\quad + \beta \left(I_{N_f^{(y)}} \otimes \left(\frac{1}{2h_x} D_{N_f^{(x)}} \right) + \left(\frac{1}{2h_y} D_{N_f^{(y)}} \right) \otimes I_{N_f^{(x)}} \right), \\
b_{ff} &= [s_{1,1}, s_{2,1}, \dots, s_{N_f^{(x)},1}, s_{1,2}, \dots, s_{N_f^{(x)},N_f^{(y)}}]^T,
\end{aligned}$$

where \otimes is the tensor product, $s_{i,j} = s(x_i, y_j)$, $(x_i, y_j) \in \Omega^{h_x, h_y}$ and

$$D_N = \begin{bmatrix} 0 & 1 & & & \\ -1 & 0 & 1 & & \\ & \ddots & \ddots & \ddots & \\ & & -1 & 0 & 1 \\ & & & -1 & 0 \end{bmatrix}_{N \times N}, \quad L_N = \begin{bmatrix} 2 & -1 & & & \\ -1 & 2 & -1 & & \\ & \ddots & \ddots & \ddots & \\ & & -1 & 2 & -1 \\ & & & -1 & 2 \end{bmatrix}_{N \times N}.$$

The other matrices and known vectors in equation (6) are defined similarly.

Remark 2.5. Since $\Omega_{i,j}^{h_x, h_y} \subset \Omega^{h_x, h_y}$, then the coefficient matrix $A_{(ij)}$ is a main diagonal sub-block of matrix A_{ff} if the same discretization scheme is applied.

3 The 2D ASDSM Algorithm

In this section, we present the ASDSM Algorithm and provide a detailed step-by-step explanation with figures. We consider the two-dimensional advection-diffusion equation, given in equation (1), with $\alpha = 1, \beta = 0$, i.e., the Poisson problem, and $g(x, y)$ and $s(x, y)$ computed from the exact solution $u(x, y) = \sin(x\pi) \sin(2y\pi)$. For the sake of clarity, we discretize the equation using a very coarse mesh with $N_f^{(x)} = N_f^{(y)} = 24$ and $N_c^{(x)} = N_c^{(y)} = 4$.

It is important to note that the inputs of the following algorithms are only the variables that change with each iteration. To improve readability, we do not include other inputs that are constant while iterating through the algorithm. Additionally, sometimes the step k can be divided into two disjoint parts that can be executed concurrently, namely substeps $k.1)$ and $k.2)$.

3.1 Computation of the initial guess

The core of our proposal is a peculiar way to compute an initial guess. This approach, outlined in Algorithm 1, consists in computing the solutions u_{fc}, u_{cf}, u_{cc} of the anisotropic and coarse linear systems in equation (6), merging together the three solutions, thus forming the approximated *coarse structure* or *skeleton* of the fine solution u_{ff} , and finally filling in the empty regions.

Algorithm 1 Initial Guess Builder

function INITIALGUESS($b_{ff}, b_{fc}, b_{cf}, b_{cc}$)

1.1) $u_{fc} = (A_{fc})^{-1} b_{fc}$

▷ Solve the equation on Ω^{h_x, H_y}

1.2) $u_{cf} = (A_{cf})^{-1} b_{cf}$

▷ Solve the equation on Ω^{H_x, h_y}

if $*b_{cc}$ is in input **then**

1.3) $u_{cc} = (A_{cc})^{-1} b_{cc}$

▷ Solve the equation on Ω^{H_x, h_y}

else

2.1) $u_{fc} = \frac{u_{fc}}{\|u_{fc}\|}$

▷ Normalize the vector

2.2) $u_{cf} = \frac{u_{cf}}{\|u_{cf}\|}$

end if

3) $\tilde{u}_{ff} = \text{Skeleton}(u_{fc}, u_{cf}, u_{cc})$

▷ Builds the skeleton of the initial guess

4) $\tilde{u}_{ff} = \text{Filler}(\tilde{u}_{ff}, b_{ff})$

▷ Fills the holes $\Omega_{i,j}^{h_x, h_y}$

return \tilde{u}_{ff}

end function

In details, in step 1), the solutions u_{fc}, u_{cf}, u_{cc} can be efficiently computed through ad-hoc solvers. For example, circulant preconditioners, incomplete LU preconditioners, and multigrid methods have already been shown to be valid

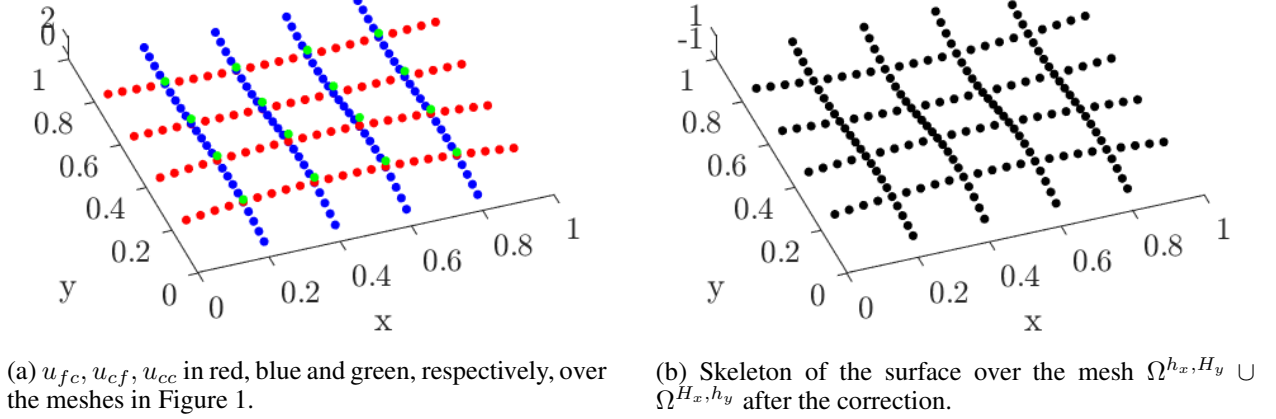


Figure 2: Coarse structure before (a) and after (b) the merging process.

preconditioners/solvers for structured anisotropic [10, 18, 8] and isotropic [9, 2, 5] linear systems. Note that, when computing the initial guess, the known term b_{cc} is in input, hence the "if" condition is satisfied. The case where u_{cc} is not provided, leading to skip step 1.3) and normalize the two solution in step 2), will be treated later. After the computation of u_{fc}, u_{cf}, u_{cc} , respectively shown in red, blue, and green in Figure 2a, in step 3) we merge them into a unique unknown \tilde{u}_{ff} through the Skeleton Builder Algorithm 2.

Algorithm 2 Skeleton Builder

```

function SKELETON( $u_{fc}, u_{cf}, u_{cc}$ )
  1.1)  $\tilde{u}_{cc}^{(1)} = P_{fc}^{cc} u_{fc}$ 
  1.2)  $\tilde{u}_{cc}^{(2)} = P_{cf}^{cc} u_{cf}$ 
  if * $u_{cc}$  is in input* then
    2)  $\hat{u}_{cc} = \text{RE}(\tilde{u}_{cc}^{(1)}, \tilde{u}_{cc}^{(2)}, u_{cc})$ 
  else
    3)  $\hat{u}_{cc} = \tilde{u}_{cc}^{(1)} \mid \hat{u}_{cc} = \tilde{u}_{cc}^{(2)}$ 
  end if
  4.1)  $e_{cc}^{(1)} = \hat{u}_{cc} - \tilde{u}_{cc}^{(1)}$ 
  4.2)  $e_{cc}^{(2)} = \hat{u}_{cc} - \tilde{u}_{cc}^{(2)}$ 
  5.1)  $\tilde{u}_{fc} = u_{fc} + \text{Spline}(e_{cc}^{(1)}, \Omega^{h_x, H_y})$ 
  5.2)  $\tilde{u}_{cf} = u_{cf} + \text{Spline}(e_{cc}^{(2)}, \Omega^{H_x, h_y})$ 
  6)  $\tilde{u}_{ff} = P_{fc}^{ff} \tilde{u}_{fc} + P_{cf}^{ff} \tilde{u}_{cf} - P_{cc}^{ff} P_{cf}^{cc} \tilde{u}_{cf}$ 
  return  $\tilde{u}_{ff}$ 
end function

```

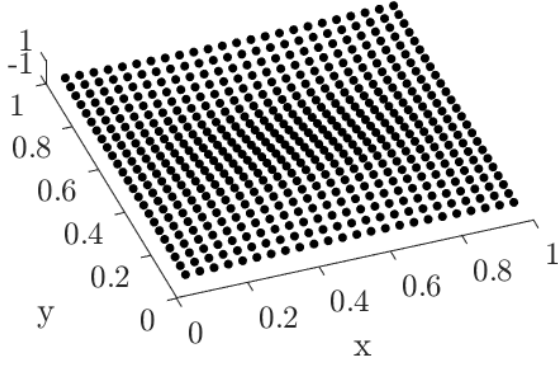
- ▷ Project the anisotropic solutions over the coarse mesh
- ▷ Richardson Extrapolation (RE) can be used
- ▷ Extrapolated coarse solution
- ▷ Choose the coarse solution
- ▷ Compute the error with respect to \hat{u}_{cc}
- ▷ Correct the two solutions

In Figure 2a we note that, due to the different meshes involved, the three solution do not perfectly overlap at the cross-points. Therefore, Algorithm 2 exploits Richardson extrapolation to compute accurate cross-points, then adjusts u_{fc} and u_{cf} , and merges them together.

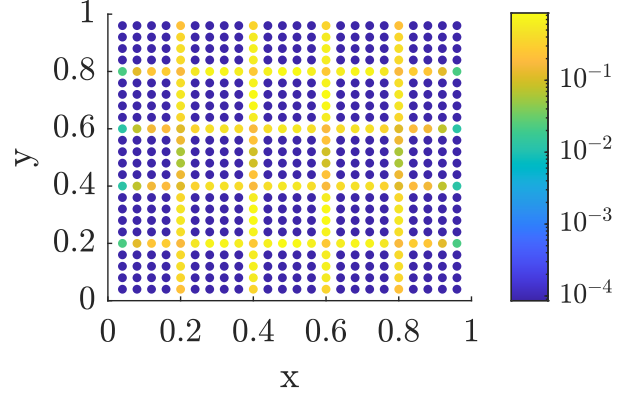
In details, in step 1) we project the two anisotropic solutions u_{fc}, u_{cf} over the coarse isotropic mesh Ω^{H_x, H_y} through the projectors P_{fc}^{cc}, P_{cf}^{cc} . Then, since u_{cc} is in input, in step 3) we use Richardson extrapolation [14] to generate a more accurate solution \hat{u}_{cc} over Ω^{H_x, H_y} .

Remark 3.1. *In order to further increase the accuracy of \hat{u}_{cc} , if the smoothness requirements are met, one can compute more solutions, cheaper than u_{fc}, u_{cf} , e.g. over the anisotropic meshes Ω^{kh_x, H_y} or Ω^{H_x, kh_y} , for some $k \in \mathbb{N}$. The more information, the higher the accuracy of the extrapolated solution.*

Now that the accurate cross-points have been computed, we have to adjust the two anisotropic solutions u_{fc}, u_{cf} into $\tilde{u}_{fc}, \tilde{u}_{cf}$ such that $P_{fc}^{cc} \tilde{u}_{fc} = P_{cf}^{cc} \tilde{u}_{cf} = \hat{u}_{cc}$, i.e., their projection onto the coarse isotropic mesh coincides with the extrapolated cross-points \hat{u}_{cc} . To do so, in step 4) we compute the distance between $P_{fc}^{cc} u_{fc}, P_{cf}^{cc} u_{cf}$ and \hat{u}_{cc} . Then, in



(a) Initial guess obtained after the filling process of the skeleton.



(b) Reshaped residual of the initial guess.

Figure 3: Initial guess (a) and respective residual (b).

step 5), we interpolate the distance with zero BCs to meshes Ω^{h_x, H_y} , Ω^{H_x, h_y} and add it to u_{fc} , u_{cf} , respectively. By using high order spline interpolation this process yields smooth unknowns \tilde{u}_{fc} , \tilde{u}_{cf} with the aforementioned property. At this point in step 6) we project the corrected anisotropic unknowns to the fine mesh Ω^{h_x, h_y} , we sum them together and finally we remove the grid points which are counted twice. The newly defined unknown \tilde{u}_{ff} is called the *skeleton* or *coarse structure* of our initial guess.

As shown in Figure 2b, the skeleton surface is zero over the so-called *empty* regions or *holes* $\Omega_{i,j}^{h_x, h_y}$ (in white) and it is smooth over the coarse structure $\Omega^{h_x, H_y} \cup \Omega^{H_x, h_y}$ (in black). This property allows for the efficient filling of the holes, as outlined in the sketch of the Filler Algorithm in 3.

Algorithm 3 Filler

function FILLER(\tilde{u}_{ff} , A_{ff} , b_{ff})

1) $c = -P_{ff}^{holes} A_{ff} \tilde{u}_{ff}$

▷ Use \tilde{u}_{ff} as BCs

2) $v = \left(P_{ff}^{holes} A_{ff} P_{holes}^{ff} \right)^{-1} \left(P_{ff}^{holes} b_{ff} + c \right)$

3) $\tilde{u}_{ff} = \tilde{u}_{ff} + P_{holes}^{ff} v$

return \tilde{u}_{ff}

end function

The filling process consists in using the skeleton \tilde{u}_{ff} as BCs for new disjoint discrete PDEs, solve them in parallel and finally update the fine unknowns.

In details, due to the zero filling of the holes, the product $A_{ff} \tilde{u}_{ff}$ in step 1) projects the information on the boundaries (the skeleton) inside the holes. Then, projector P_{ff}^{holes} removes the skeleton from c by only keeping the empty regions, which now include the information regarding the boundaries. Hence, vector c contains the BCs for the linear system defined over the holes.

In step 2) we project matrix A_{ff} and the known term b_{ff} over the fine mesh without the skeleton. The solution of the newly obtained linear system is the chaining of the solutions inside each one of the holes.

Note that matrix $P_{ff}^{holes} A_{ff} P_{holes}^{ff}$ has a block structure. According to Remark 2.5, since the same discretization scheme is used, each block of $P_{ff}^{holes} A_{ff} P_{holes}^{ff}$ corresponds to $A_{(ij)}$ for some i, j . Therefore, the inversion of the projected matrix can be easily parallelized.

Finally, in step 3) we update the skeleton with the new information. As shown in Figure 3a, this process yields a continuous unknown (unless the time variable is involved).

Before giving the ASDSM algorithm, we summarize three properties of the Initial Guess Algorithm 1.

Proposition 3.2. *Let $u_{ff} = (A_{ff})^{-1} b_{ff}$ be the numerical solution to the fine linear system in equation (6) and let $u^{(0)}$ be the initial guess computed through Algorithm 1, with r being the residual vector reshaped into a discrete surface. Then*

- 1) *the unknown $u^{(0)}$ coincides with u_{ff} if and only if the skeleton of $u^{(0)}$ coincides with the skeleton of u_{ff} ;*

- 2) r is zero over the holes and non-zero over its skeleton, unless $u^{(0)} = u_{ff}$;
- 3) The skeleton of r may be non-smooth near the coarse mesh points Ω^{H_x, H_y} , i.e., the cross-points of the two anisotropic meshes.

Proof. Statement 1) If $u^{(0)}$ coincides with u_{ff} , clearly the two skeletons coincide. Conversely, if the two skeletons coincide then the output of Algorithm 2 is

$$\tilde{u}_{ff} = \left(I - P_{holes}^{ff} P_{holes}^{holes} \right) u_{ff}, \quad (7)$$

i.e., $\tilde{u}_{ff} = 0$ over the holes $\Omega_{holes}^{h_x, h_y}$ and $\tilde{u}_{ff} = u_{ff}$ over the skeleton $\Omega^{h_x, H_y} \cup \Omega^{H_x, h_y}$. Then \tilde{u}_{ff} passes through Algorithm 3 yielding

$$u^{(0)} = \tilde{u}_{ff} + P_{holes}^{ff} \left(P_{holes}^{holes} A_{ff} P_{holes}^{ff} \right)^{-1} \left(P_{holes}^{holes} b_{ff} - P_{holes}^{holes} A_{ff} \tilde{u}_{ff} \right),$$

and from equation (7)

$$\begin{aligned} u^{(0)} &= \tilde{u}_{ff} + P_{holes}^{ff} \left(P_{holes}^{holes} A_{ff} P_{holes}^{ff} \right)^{-1} \left(P_{holes}^{holes} A_{ff} P_{holes}^{ff} P_{holes}^{holes} u_{ff} \right) \\ &= \tilde{u}_{ff} + P_{holes}^{ff} P_{holes}^{holes} u_{ff}, \end{aligned}$$

which is equal to u_{ff} and proves statement 1).

Statement 2) This is a consequence of Remark 2.5. Indeed, consider $P_{ff}^{holes} r$, i.e., the projection of the residual over $\Omega_{holes}^{h_x, h_y}$. Then, we have

$$\begin{aligned} P_{ff}^{holes} r &= P_{ff}^{holes} \left(b_{ff} - A_{ff} u^{(0)} \right) \\ &= P_{ff}^{holes} \left(b_{ff} - A_{ff} \left(\tilde{u}_{ff} + P_{holes}^{ff} v \right) \right) \\ &= P_{ff}^{holes} \left(b_{ff} - A_{ff} \left(\tilde{u}_{ff} + P_{holes}^{ff} \left(P_{holes}^{holes} A_{ff} P_{holes}^{ff} \right)^{-1} \left(P_{holes}^{holes} b_{ff} + c \right) \right) \right) \\ &= P_{ff}^{holes} b_{ff} - P_{ff}^{holes} A_{ff} \tilde{u}_{ff} - P_{ff}^{holes} A_{ff} P_{holes}^{ff} \left(P_{holes}^{holes} A_{ff} P_{holes}^{ff} \right)^{-1} \left(P_{holes}^{holes} b_{ff} + c \right) \\ &= P_{ff}^{holes} b_{ff} - P_{ff}^{holes} A_{ff} \tilde{u}_{ff} - P_{ff}^{holes} b_{ff} - c \end{aligned}$$

which is zero since $c = -P_{ff}^{holes} A_{ff} \tilde{u}_{ff}$. Hence, the residual over the holes is zero. Moreover, in the case where $u^{(0)} \neq u_{ff}$, the residual is non-zero and by the previous result it must be non-zero only over its skeleton.

Statement 3) It follows by the fact that the coarse points $(x_i, y_j) \in \Omega^{h_x, h_y} \cap \Omega^{H_x, H_y}$ are the cross points between 4 subdomains $\Omega_{i,j}^{h_x, h_y}$ for some i, j , where 4 solution are computed through the wrong BCs, since $u^{(0)} \neq u_{ff}$. Therefore, if (x_i, y_j) is a cross-point between the two anisotropic meshes, there may be a significant difference between $r_{i,j}$ (calculated from elements of the skeleton only) and $r_{i\pm 1, j}$ or $r_{i, j\pm 1}$ (calculated from elements of two domains). \square

Remark 3.3. *In the proof of Proposition 3.2, there is no explicit connection established between the structure of the residual and the discretization method used for the anisotropic linear systems. As a result, using an alternative discretization scheme would still yield a residual with the same sparse structure.*

3.2 Iterative approach

The ASDSM Algorithm, summarized in Algorithm 4, consists in iterating the Initial Guess Algorithm 1 by exploiting the structure of the residual.

After the computation of the initial guess, we compute the residual and iteratively apply corrections using Algorithm 1 to provide an initial guess of the error.

In details, we compute the residual in step 3) and observe that, as shown in Proposition 3.2 and depicted in Figure 3b, it is concentrated on the skeleton of the solution. Therefore, in step 4) we project the residual into the anisotropic meshes Ω^{h_x, H_y} and Ω^{H_x, h_y} using the projectors P_{ff}^{fc} and P_{ff}^{cf} , shown in Figures 4a and 4a, respectively. In step 5) we compute an approximate solution \tilde{e}_{ff} of the error equation $A_{ff} e_{ff} = r_{ff}$ through the Initial Guess Algorithm 1.

Algorithm 4 ASDSM Algorithm

function ASDSM

1) $u^{(0)} = \mathbf{InitialGuess}(b_{ff}, b_{fc}, b_{cf}, b_{cc})$

▷ Compute the initial guess

2) $k = 0$
while $\|b_{ff} - A_{ff}u^{(k)}\| < \text{tol}$ | *residual stagnates* **do**

3) $r_{ff} = b_{ff} - A_{ff}u^{(k)}$

▷ Compute the residual on Ω^{h_x, h_y}

4.1) $r_{fc} = P_{ff}^{fc} r_{ff}$

▷ Project the residual into Ω^{h_x, H_y}

4.2) $r_{cf} = P_{ff}^{cf} r_{ff}$

▷ Project the residual into Ω^{H_x, h_y}

5) $\tilde{e}_{ff} = \mathbf{InitialGuess}(0 \cdot b_{ff}, r_{fc}, r_{cf})$

▷ Approximate the error

6) $\hat{s} = \arg \min_{s \in \mathbb{R}^+} \|b_{ff} - A_{ff}(u^{(k)} + s\tilde{e}_{ff})\|$

7) $u^{(k+1)} = u^{(k)} + \hat{s}\tilde{e}_{ff}$

▷ Apply the scaled correction

8) $k = k + 1$
end while
return $u^{(k)}$
end function

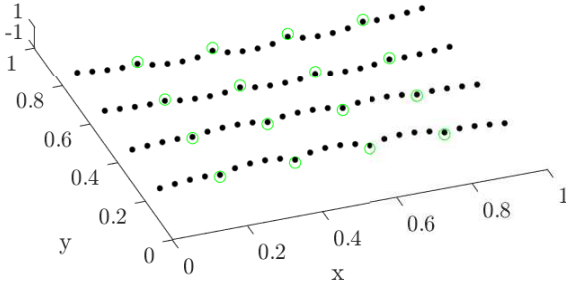
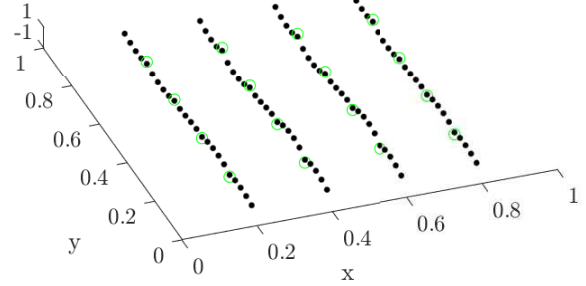

(a) r_{fc} : residual r_{ff} projected over the mesh Ω^{h_x, H_y} .

(b) r_{cf} : residual r_{ff} projected over the mesh Ω^{H_x, h_y} .

Figure 4: Residual projected over the two anisotropic meshes.

However, we face two challenges in this process: the residual is not smooth enough to allow for the use of Richardson extrapolation, and the different scalings of the two anisotropic error equations $A_{fc}e_{fc} = r_{fc}$ and $A_{cf}e_{cf} = r_{cf}$ may lead to large differences in the norms of the solutions e_{fc} and e_{cf} . Indeed, we observe that, as reported in Proposition 3.2 and depicted in Figures 4a and 4b, the residual surfaces show irregularities which lie close to the coarse mesh points of Ω^{H_x, H_y} (green), i.e., the cross points of the two anisotropic meshes. Moreover, looking at the z -axis in Figures 5a,5b we observe a slight difference in scale, which could get larger when increasing the mesh points.

Therefore, to address these issues, in step 3) of Algorithm 2, we randomly choose between $P_{fc}^{cc}u_{fc}$ and $P_{cf}^{cc}u_{cf}$ as \hat{u}_{cc} , since \hat{u}_{cc} cannot be extrapolated, while, in step 2) of Algorithm 1, we normalize the two solutions before constructing the skeleton. The normalization ensures that the two coarse solutions, which are both sub-samples of a finer solution, have approximately the same norm.

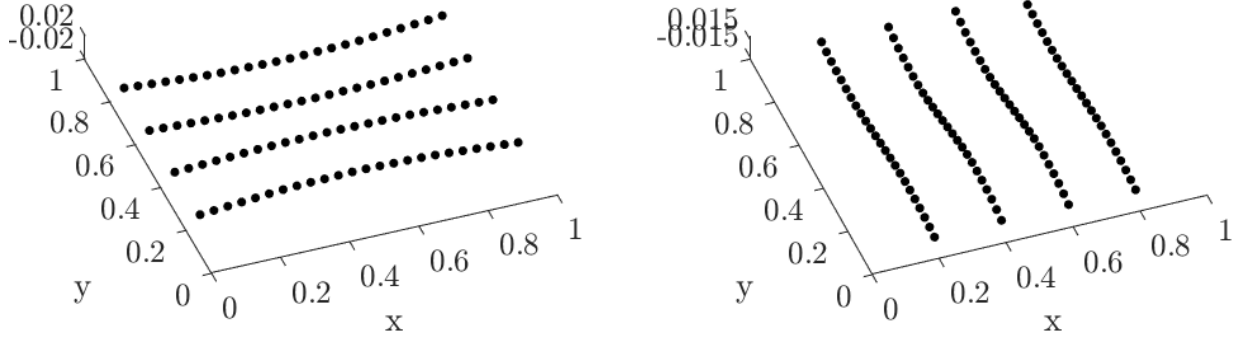
In the final step 6) of the main algorithm, we compute an optimal scaling of the update \tilde{e}_{ff} such that it minimizes the residual. This step is needed to correctly scale the solution after the normalization and it is crucial to ensure a non-increasing residual.

Remark 3.4. *The scaling applied in step 7) of the ASDSM Algorithm 4 ensures that the algorithm cannot diverge, but it does not prevent stagnation. Moreover, since the error is computed through Algorithm 1, we infer that Proposition 3.2 holds true also for $u^{(k)}$, $\forall k \geq 0$.*

3.3 Efficient implementation

In order to efficiently implement ASDSM, the following remarks should be considered.

- The sparsity of the residual can be leveraged to decrease the computational cost by restricting the computations to the non-zero elements only;


(a) e_{fc} : error computed over the mesh Ω^{h_x, H_y} .

(b) e_{cf} : error computed over the mesh Ω^{H_x, h_y} .

Figure 5: Solutions of the two anisotropic error equations.

- The computation of \hat{s} , which requires to solve an over-determined linear system with one unknown and $O(N_c^{(x)} N_f^{(x)} + N_c^{(y)} N_f^{(y)})$ equations, can be made more efficient by considering a random subset of equations, rather than all of them;
- When computing the initial guess of the error, the filling process consists in solving many homogeneous PDEs concurrently. In some cases the solution of a homogeneous PDE can be found analytically, and this would essentially allow to eliminate the cost of the filling process;
- The inversion of the block matrix in Step 2) of Algorithm 3 can be done through matrix free approaches [15];
- As a consequence of Proposition 3.2, smart memory management can be used to reduce the storage requirements for the iterative unknown $u^{(k)}$ by only storing the skeleton and elements close to it, rather than all $N_f^{(x)} N_f^{(y)}$ components. This can bring the storage requirements down to $O(N_c^{(x)} N_f^{(y)} + N_c^{(y)} N_f^{(x)})$.

3.4 Extension to different discretizations and PDEs

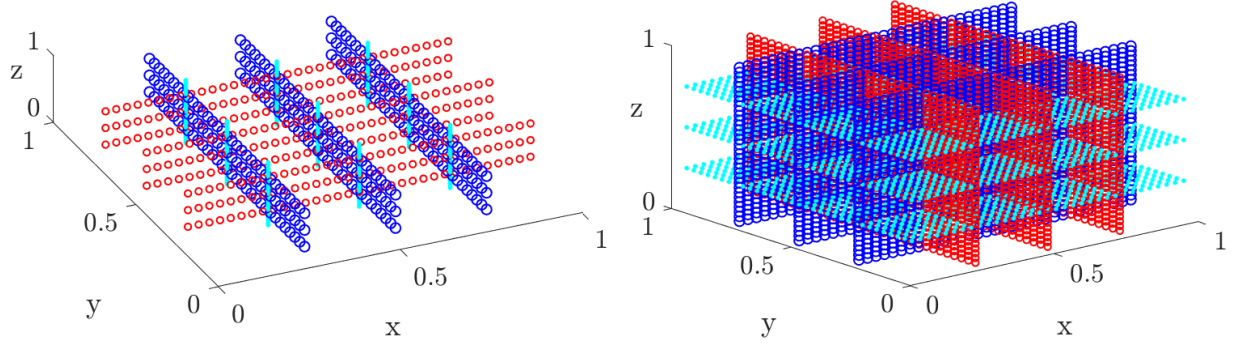
In case of higher order PDEs or higher accuracy order of the discretization schemes, the discretization process would yield banded coefficient matrices with bandwidth larger than 3, and a consequent increase in BCs. This can create difficulties in properly filling the holes $\Omega_{holes}^{h_x, h_y}$, as the linear system obtained from the discretization of the PDE over each hole may require more than one BC. One potential solution is to use different discretization methods near the edges of the domain. For example, through the Taylor expansion we obtain the following 3-rd order accurate finite difference discretizations of the second order derivative

$$\begin{aligned}
u''(x_i) &= \frac{-u_{i-2} + 16u_{i-1} - 30u_i + 16u_{i+1} - u_{i+2}}{12h^2} + O(h^3); \\
u''(x_i) &= \frac{10u_{i-1} - 15u_i - 4u_{i+1} + 14u_{i+2} - 6u_{i+3} + u_{i+4}}{12h^2} + O(h^3); \\
u''(x_i) &= \frac{u_{i-4} - 6u_{i-3} + 14u_{i-2} - 4u_{i-1} - 15u_i + 10u_{i+1}}{12h^2} + O(h^3).
\end{aligned}$$

Therefore, we could define the linear systems in the holes through the above equalities such that only one BC is required. Then, to ensure that Remark 2.5 holds true, we build the fine coefficient matrix A_{ff} such that its sub-blocks coincide with the linear systems in the holes. Since Remark 2.5 is essential to the proof of Proposition 3.2, it is then theoretically possible to extend ASDSM towards higher order PDEs or higher order accuracy discretization schemes.

3.5 Extension to the 3D case

In the 3D case, we aim to solve PDE (1) over a fine 3D uniform mesh. By extending the notation introduced in Section 2.1, we denote such mesh by Ω^{h_x, h_y, h_z} , with h_x, h_y, h_z being the grid widths in each dimension. An optimal way to extend ASDSM would be to discretize the PDE over four different meshes: three strongly anisotropic meshes $\Omega^{H_x, h_y, h_z}, \Omega^{h_x, H_y, h_z}, \Omega^{h_x, h_y, H_z}$ and one coarse isotropic mesh Ω^{H_x, H_y, H_z} . However, as illustrated in Figure 6a, the problem lies in the nested meshes. In this case, the cubic empty regions only have of 8 grid points as BC, i.e., the



(a) Meshes Ω^{h_x, H_y, H_z} in red, Ω^{H_x, h_y, H_z} in blue, Ω^{H_x, H_y, h_z} in cyan. (b) Meshes Ω^{H_x, h_y, h_z} in red, Ω^{h_x, H_y, h_z} in blue, Ω^{h_x, h_y, H_z} in cyan.

Figure 6: Different choice of the anisotropic meshes.

corners of the cube, and there is no solution provided in the faces. Therefore, the obtained skeleton cannot be used as BC for new disjoint subproblems.

One potential solution is to consider the denser anisotropic meshes, such as Ω^{H_x, h_y, h_z} , Ω^{h_x, H_y, h_z} , Ω^{h_x, h_y, H_z} . In Figure 6b, it can be observed that the use of denser meshes results in well-defined BCs for the disjoint subproblems within the holes. However, it is important to note that this approach also leads to a significant increase in computational cost due to the increased density of the meshes.

In the numerical results section, when addressing the 3D case, we will implement ASDSM by iterating over the meshes Ω^{H_x, h_y, h_z} , Ω^{h_x, H_y, h_z} , Ω^{h_x, h_y, H_z} with Ω^{H_x, H_y, H_z} as the coarse intersection mesh. Note that, unlike the 2D case, the mesh Ω^{H_x, H_y, H_z} does not contain all the intersection points among the previous meshes. For example, $\Omega^{h_x, H_y, H_z} = \Omega^{h_x, h_y, H_z} \cap \Omega^{h_x, H_y, h_z}$. Therefore, in order to ensure a well-defined merging process, we also extrapolate the other intersection points.

4 Numerical results

This section presents numerical results evaluating the performance of ASDSM. The implementation is in Matlab 2020b and the tests are run on a machine with AMD Ryzen 5950X processor and 64GB of RAM.

The algorithms used in this section are available in [17]. In the following examples, we set $N_c^{(x)} = N_c^{(y)} = N_c^{(z)} = N_c$ and $N_f^{(x)} = N_f^{(y)} = N_f^{(z)} = N_f$. Moreover, each example will tests ASDSM for solving (1) or (2) under two scenarios: one where the solution is smooth, and the second with an oscillatory solution. As a results, we use the notation $r_k^{(1)}, r_k^{(2)}$ to represent the residual at the k -th iteration of ASDSM for solving the PDE under the first and second scenarios, respectively. Note that, when $k = 0$, $r_0^{(j)}$, $j = 1, 2$ represents the residual of the initial guess computed through Algorithm 1.

Example 1: Here we test ASDSM for solving the two-dimensional steady state advection-diffusion equation (1) with the following settings:

- 1) $\alpha_1 = \alpha_2 = \beta_1 = \beta_2 = 1$ and functions s, g computed from the exact solution $u(x, y) = \sin(x\pi + y\pi)$;
- 2) $\alpha_1 = 1 + x^2$, $\alpha_2 = 2 + xy$, $\beta_1 = 2 - x$, $\beta_2 = 1 + y$ and functions s, g computed from the exact solution $u(x, y) = \sin(4x\pi + 4y\pi)$.

We note that settings 1) and 2) differ from the choice of coefficients α_i, β_i , which in 1) are constants and equal, and in 2) they are taken as positive functions. Additionally, the solution in setting 2) is more oscillatory than in setting 1), making the problem harder to solve, especially in the case of extremely anisotropic meshes, as more points are needed to better approximate the solution.

Figures 7a and 7b, respectively, show the residuals $r_k^{(1)}, r_k^{(2)}$ at the iteration $k = 0, \dots, 20$ for the two settings described above. The dotted, dashed and circled lines represent $N_c = 5, 10, 20$ respectively, while the red, green, blue and magenta lines represent $N_f = 400, 800, 1600, 3200$. In each case, the size of the linear system being solved is $N_f \times N_f$, therefore, different type of lines with the same color represent the residual of ASDSM while solving the

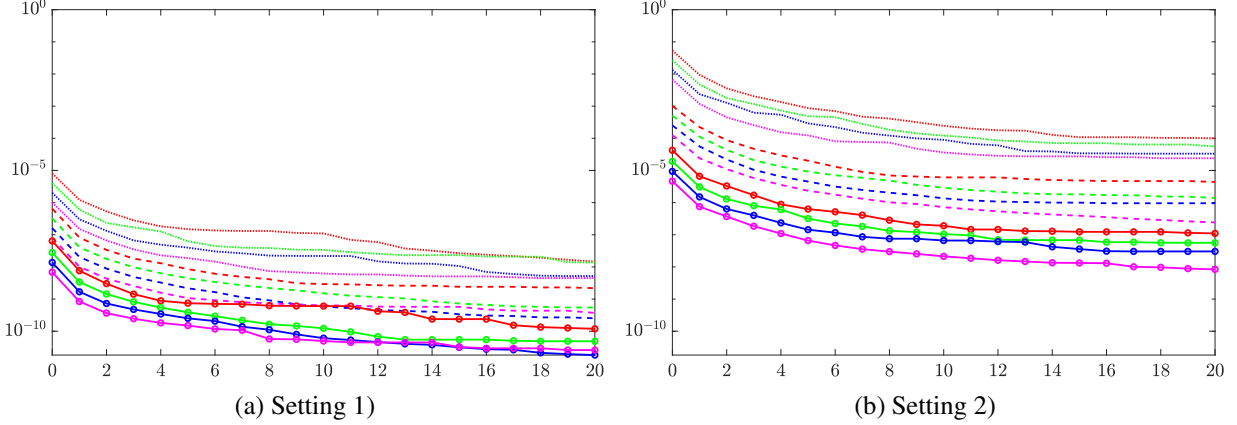


Figure 7: Residuals $r_k^{(1)}, r_k^{(2)}$ at each iteration of ASDSM applied to equation (1) for the two settings. The dotted, dashed and circled lines represent $N_c = 5, 10, 20$ respectively, while the red, green, blue and magenta lines represent $N_f = 400, 800, 1600, 3200$.

same linear system. This is because N_c is only needed in ASDSM to define the size of the anisotropic linear systems. Hence, larger N_c leads to a more computationally expensive iteration of ASDSM.

In Figures 7a, where setting 1) is considered, it can be observed that the Richardson extrapolation inside the initial guess algorithm leads to a strong initial boost, resulting in a very small $r_0^{(1)}$ for every combination of N_c, N_f . Then, the first iteration of ASDSM further strongly reduce the residual by approximately one order of magnitude. However, after the first iteration, the reduction factor decreases and seems to converge to 1 as k increases, leading to stagnation. One possible cause for this is the low accuracy of the anisotropic linear system. As ASDSM gets closer to the solution, the initial guess of the error becomes less and less accurate. Indeed, we note that by fixing N_f and increasing N_c , i.e., reducing the anisotropy and increasing accuracy at the same time, the stagnation point lowers. Another cause may be related to the smoothness of the residual (see Example 2 for further details).

Furthermore, when fixing N_c and increasing N_f , which increases the anisotropy, the stagnation point still appears to decrease. This suggests that increasing the size of main linear system, and consequently the accuracy of its solution, improves the performance of ASDSM.

When considering setting 2), in Figure 7b we note a similar behavior of $r_k^{(2)}$ with respect to $r_k^{(1)}$. The main difference lies in the starting point at $k = 0$. In this case, of an oscillatory solution, the extrapolated cross-points are less accurate than in the previous case. Therefore, the initial guess algorithm yields a less accurate solution. Another loss of accuracy may come from the use of variable coefficients $\alpha_i, \beta_i, i = 1, 2$ in place of constant ones used in setting 1). Indeed, when $N_c = 5$ the residual $r_0^{(1)}$ is almost 4 orders of magnitude smaller than $r_0^{(2)}$, and 3 orders of magnitude when $N_c = 10, 20$.

Example 2: In this example we show an important drawback of ASDSM, which consists in making the residual highly irregular at the coarse points. Consider the following two toy problems:

- 1) 2-dimensional space steady state advection diffusion equation (1) with $\alpha_i = \beta_i = 1, i = 1, 2$ and s, g computed from the exact solution $u(x, y) = \sin(x\pi + y\pi)$;
- 2) 1-dimensional space time-dependent advection diffusion equation (2) with $\alpha_1 = \beta_1 = 1$ and s, g computed from the exact solution $u(x, t) = \sin(x\pi + t\pi)$.

In Figure 8 we show the reshaped residual obtained after iterating ASDSM 20 times, i.e., when ASDSM stagnates. In both cases, strong irregularities can be observed at the coarse points. In the time-dependent case, less severe irregularities are also observed along the mesh dense in time Ω^{H_x, h_t} . This results in highly irregular projected residuals in steps 4.1) and 4.2) of the ASDSM Algorithm 4, leading to inaccurate solutions in steps 1.1) and 1.2) of Algorithm 1 which in turn causes the stagnation.

Additional tests, not presented in this paper, have shown that an artificial smoothing of the residual reduces the stagnation point.

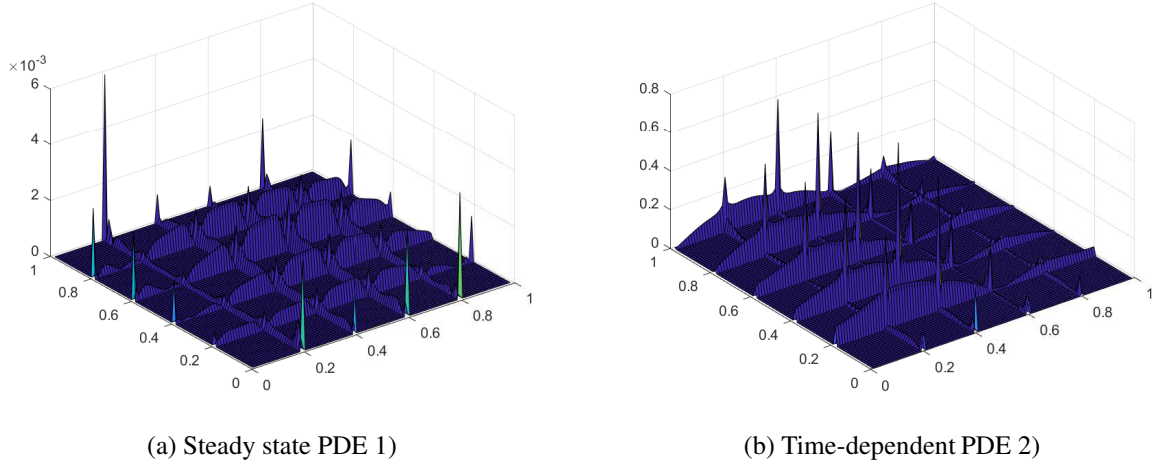


Figure 8: Reshaped absolute residual after 20 iterations of ASDSM

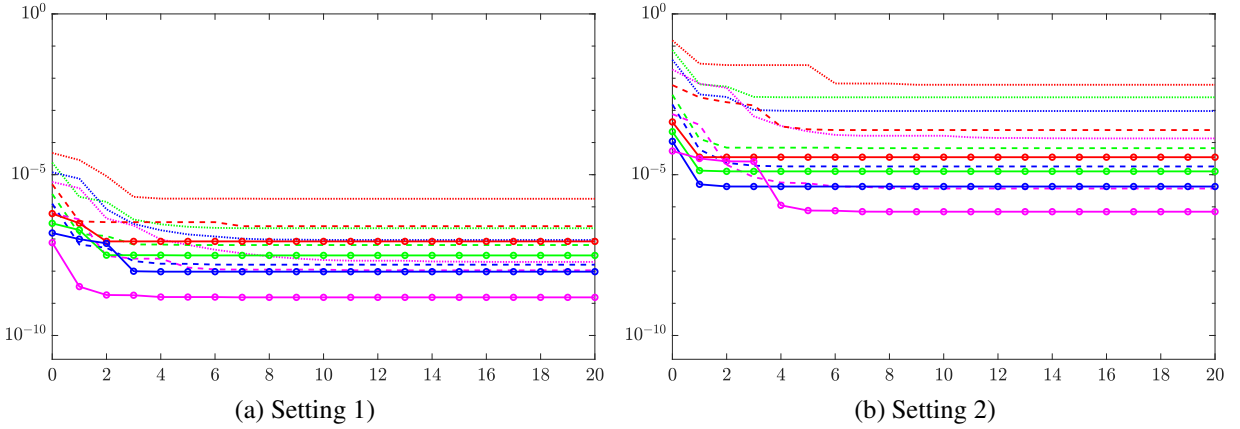


Figure 9: Residuals $r_k^{(1)}, r_k^{(2)}$ at each iteration of ASDSM applied to equation (2) for the two settings. The dotted, dashed and circled lines represent $N_c = 5, 10, 20$ respectively, while the red, green, blue and magenta lines represent $N_f = 400, 800, 1600, 3200$.

Example 3: Here we test ASDSM for solving the one-dimensional space time-dependent advection-diffusion equation (2) with the following settings:

- 1) $\alpha_1 = \beta_1 = 1$ and functions s, g computed from the exact solution $u(x, t) = \sin(x\pi + t\pi)$;
- 2) $\alpha_1 = 1 + x^2, \beta_1 = 2 - x$ and functions s, g computed from the exact solution $u(x, t) = \sin(4x\pi + 4t\pi)$.

Note that the two settings, which involve a smooth and an oscillatory solution, are the same as in Example 1, but with the variable t replacing y .

With the same notation as in Example 1, Figures 9a and 9b show the absolute residuals $|r_k^{(1)}|, |r_k^{(2)}|$ at the k -th iteration, respectively. A comparison between Figures 9 and 7 shows that, in general, the same observations made in Example 1 apply to this time-dependent case as well. However, the main difference is in the trend of the residual, which in Figure 9 is shown to be less smooth than in Figure 7. The reason for such behavior lies in step 3) of the Skeleton builder Algorithm 2, where the cross-points of the error surface cannot be extrapolated, and a random solution is taken as “the most accurate”. In this case, the solution e_{H_x, h_t} computed over the dense in time mesh Ω^{H_x, h_t} is more accurate than e_{h_x, H_t} computed over the dense in space mesh Ω^{h_x, H_t} . Therefore, when the randomly chosen cross-points are the ones of error e_{H_x, h_t} , the residual strongly reduces. However, this large reduction in residual only seems to happen a couple of times before stagnation occurs for the same reasons reported in Example 1.

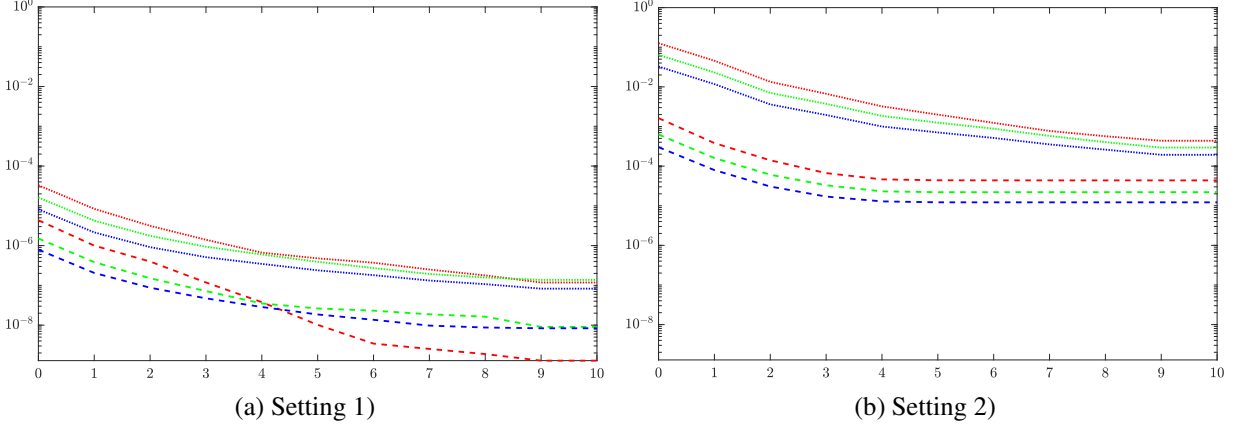


Figure 10: Residuals $r_k^{(1)}, r_k^{(2)}$ at each iteration of ASDSM applied to equation (1) for the two settings. The dotted, dashed lines represent $N_c = 5, 10$ respectively, while the red, green, blue and magenta lines represent $N_f = 70, 150, 300$.

Example 4: Here we test ASDSM for solving three-dimensional steady state advection-diffusion equation (1) with the following settings:

- 1) $\alpha_i = \beta_i = 1$, $i = 1, 2, 3$ and functions s, g are computed from the exact solution $u(x, y, z) = \sin(x\pi + y\pi + z\pi)$;
- 2) $\alpha_1 = 1 + x^2$, $\alpha_2 = 2 + xy$, $\alpha_3 = 3 - xyz$, $\beta_1 = 2 - x$, $\beta_2 = 1 + y$, $\beta_3 = 2 - x + yz$ and functions s, g are computed from the exact solution $u(x, t) = \sin(4x\pi + 4y\pi + 4z\pi)$.

The smooth and oscillatory solutions of settings 1) and 2) are extensions of the settings in Exercise 1, with the addition of the time variable t . In Figures 10a, 10b we respectively show the residuals $r_k^{(1)}, r_k^{(2)}$ at the k -th iteration of ASDSM applied to PDE (1) with settings 1) and 2). To reduce the computational time of the tests, the results for $N_c = 20$, previously reported as the circled line, are not provided and the study is restricted to $N_f \in \{70, 150, 300\}$, represented by colors red, green and blue, respectively.

From Figure 10 we can observe that even though the 3-dimensional case is more complex from an algorithmic point of view, and also involves more cross-points, the behavior of the residual is similar to that of Example 1. Therefore, the same observations apply and it is expected that similar results will be obtained for higher values of N_c, N_f .

5 Conclusions

The ASDSM Algorithm opens a new window on methods based on structured sparse residuals. These preliminary results show that, by decomposing the problem into disjoint sub-problems and merging the solutions, we are able to effectively reduce the dimensionality of the problem by 1 and improve computational efficiency. While further research is needed to address issues such as convergence and optimal choice of coarse points, the ASDSM algorithm has the potential to be a valuable tool for tackling large linear systems as solver or by providing a good initial guess for other iterative solvers, e.g., Domain Decomposition methods. It may also be used to provide a fast solution for shooting methods, which do not always require a high accuracy.

In future work, we will explore alternatives to overcome the limitations of the current algorithm, as well as examine its potential application to non-linear problems and unstructured meshes.

Acknowledgments

This research was supported by the EuroHPC TIME-X project n. 955701.

References

- [1] H. Bungartz, M. Griebel, *Sparse grids*, Acta Numerica, Vol. 13, p. 147-269, 2004.

- [2] S. Doi, *On parallelism and convergence of incomplete LU factorizations*, Applied Numerical Mathematics, Vol. 7.5, p. 417-436 (1991).
- [3] L. Formaggia, S. Micheletti, S. Perotto, (Anisotropic mesh adaptation in computational fluid dynamics: application to the advection-diffusion-reaction and the Stokes problems), Applied Numerical Mathematics, Vol. 51, p. 511-533 (2004).
- [4] M.J. Gander, J. Liu, S.L. Wu, X. Yue, T. Zhou, *Paradiag: Parallel-in-time algorithms based on the diagonalization technique*, arXiv preprint arXiv:2005.09158 (2020).
- [5] W. Hackbusch, *Multi-grid methods and applications*, Springer Science & Business Media Vol. 4, 2013.
- [6] J. Han, A. Jentzen, E. Weinan, *Solving high-dimensional partial differential equations using deep learning*, Proceedings of the National Academy of Sciences 115.34, p. 8505-8510 (2018).
- [7] C. Huré, H. Pham, X. Warin, *Deep backward schemes for high-dimensional nonlinear PDEs*, Mathematics of Computation 89.324, p. 1547-1579 (2020).
- [8] J. van Lent, S. Vandewalle, *Multigrid Waveform Relaxation for Anisotropic Partial Differential Equations*, Springer, Numerical Algorithms 31, p. 361-380 (2002).
- [9] I.D. Lirkov, S.D. Margenov, P.S. Vassilevski, *Circulant block-factorization preconditioners for elliptic problems*, Springer, Computing 53, p. 59-74 (1994).
- [10] I.D. Lirkov, S.D. Margenov, L.T. Zikatanov, *Circulant block-factorization preconditioning of anisotropic elliptic problems*, Springer, Computing 58, p. 245-258 (1997).
- [11] Z. Liu, W. Cai, Z.Q.J. Xu, *Multi-Scale Deep Neural Network (MscaleDNN) for Solving Poisson-Boltzmann Equation in Complex Domains*, Communications in Computational Physics, Vol. 28, Number 5, p. 1970-2001 (2020).
- [12] I.G. Lisle, S.L.T. Huang, G.J. Reid, *Structure of symmetry of PDE: exploiting partially integrated systems*, Proceedings of the 2014 Symposium on Symbolic-Numeric Computation (2014).
- [13] M.M. Rahaman, H. Takia, Md.K. Hasan, Md.B. Hossain, S. Mia, and K. Hossen, *Application of Advection Diffusion Equation for Determination of Contaminants in Aqueous Solution: A Mathematical Analysis*, Applied Mathematics and Physics, vol. 10, Number 1 (2022).
- [14] S.A. Richards, *Completed Richardson extrapolation in space and time*, Communications in numerical methods in engineering, Vol. 13.7, p. 573-582 (1997).
- [15] J. Schäfer, X. Huang, S. Kopecz, P. Birken, M.K. Gobbert, A. Meister, *A memory-efficient finite volume method for advection-diffusion-reaction systems with nonsmooth sources*, Numerical Methods for Partial Differential Equations, Vol. 31, Number 1, p. 143-167 (2015).
- [16] R.N. Singh, (Advection diffusion equation models in near-surface geophysical and environmental sciences), J. Ind. Geophys. Union, Vol. 17, Number 2, p. 117-127 (2013).
- [17] K. Trotti, ASDSM Algorithms 2D and 3D, <https://github.com/ken13889/ASDSM>
- [18] S.A. Vinogradova, L.A. Krukier, *The use of incomplete LU decomposition in modeling convection-diffusion processes in an anisotropic medium*, Mathematical Models and Computer Simulations, Vol. 5.2, p. 190-197 (2013).
- [19] X. Warin, *Nesting Monte Carlo for high-dimensional non-linear PDEs*, Monte Carlo Methods and Applications 24.4, p. 225-247 (2018).
- [20] E. Weinan, J. Han, A. Jentzen, *Algorithms for solving high dimensional PDEs: from nonlinear Monte Carlo to machine learning*, Nonlinearity 35.1, Number 278 (2021).